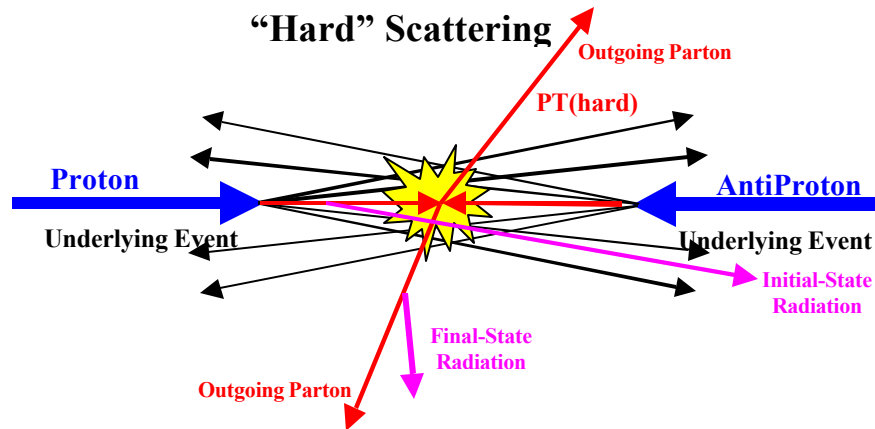
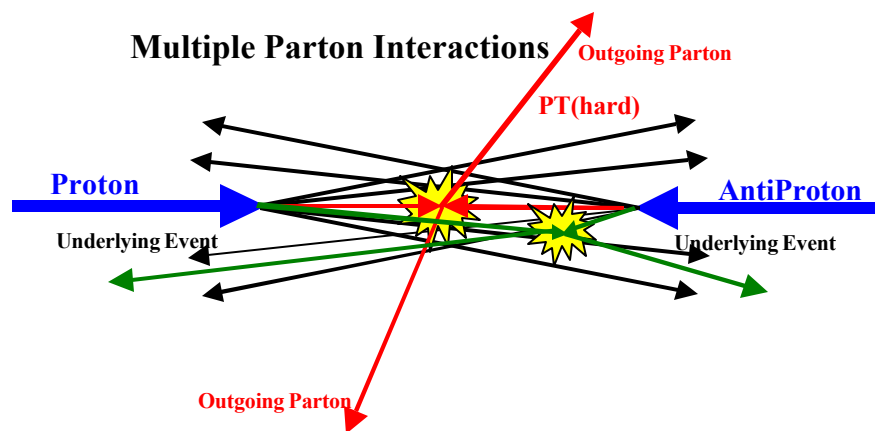


# The Underlying Event in Hard Scattering Processes



**Fig. 1.** Illustration of a proton-antiproton collision in which a “hard” 2-to-2 parton scattering with transverse momentum,  $P_T(\text{hard})$ , has occurred. The resulting event contains particles that originate from the two outgoing partons (plus final-state radiation) and particles that come from the breakup of the proton and antiproton (*i.e.* “beam-beam remnants”). The “underlying event” consists of the beam-beam remnants plus initial-state radiation.



**Fig. 2.** Illustration of a proton-antiproton collision in which a multiple parton interaction has occurred. In addition to the “hard” 2-to-2 parton scattering with transverse momentum,  $P_T(\text{hard})$ , there is an additional “semi-hard” parton-parton scattering that contributes particles to the “underlying event”. For Pythia, we include the contributions from multiple parton scattering in the beam-beam remnant component.

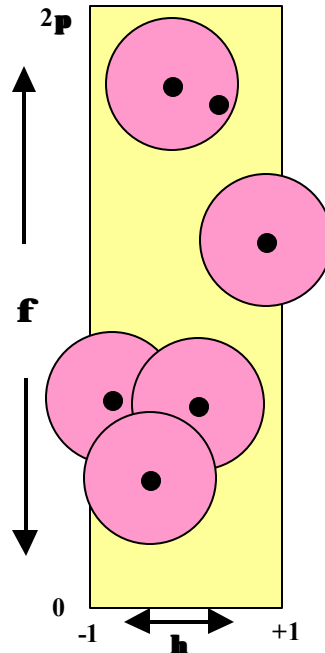


Fig. 3. Illustration of an event with six charged particles ( $P_T > 0.5$  GeV and  $|\eta| < 1$ ) and five charged “jets” (circular regions in  $\eta$ - $\phi$  space with  $R = 0.7$ ).

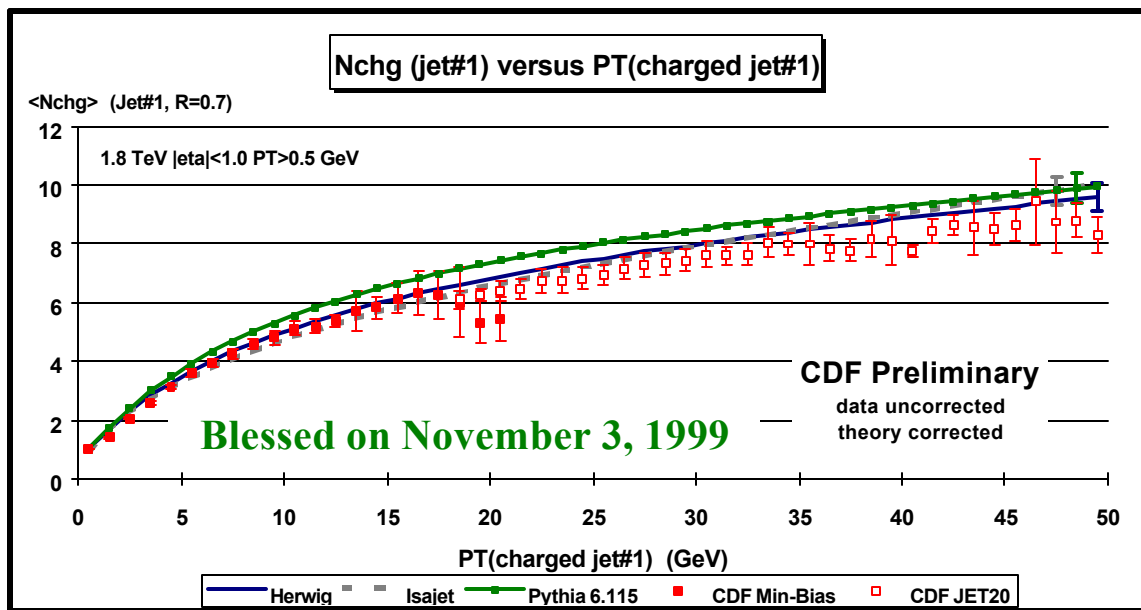


Fig. 4. Plot shows the average number of charged particles ( $P_T > 0.5$  GeV,  $|\eta| < 1$ ) within the leading charged jet ( $R = 0.7$ ) as a function of the  $P_T$  of the leading charged jet. The solid (open) points are Min-Bias (JET20) data. The errors on the (uncorrected) data include both statistical and correlated systematic uncertainties. The QCD “hard scattering” theory curves (Herwig 5.9, Isajet 7.32, Pythia 6.115) are corrected for the track finding efficiency and have an error (statistical plus systematic) of around 5%.

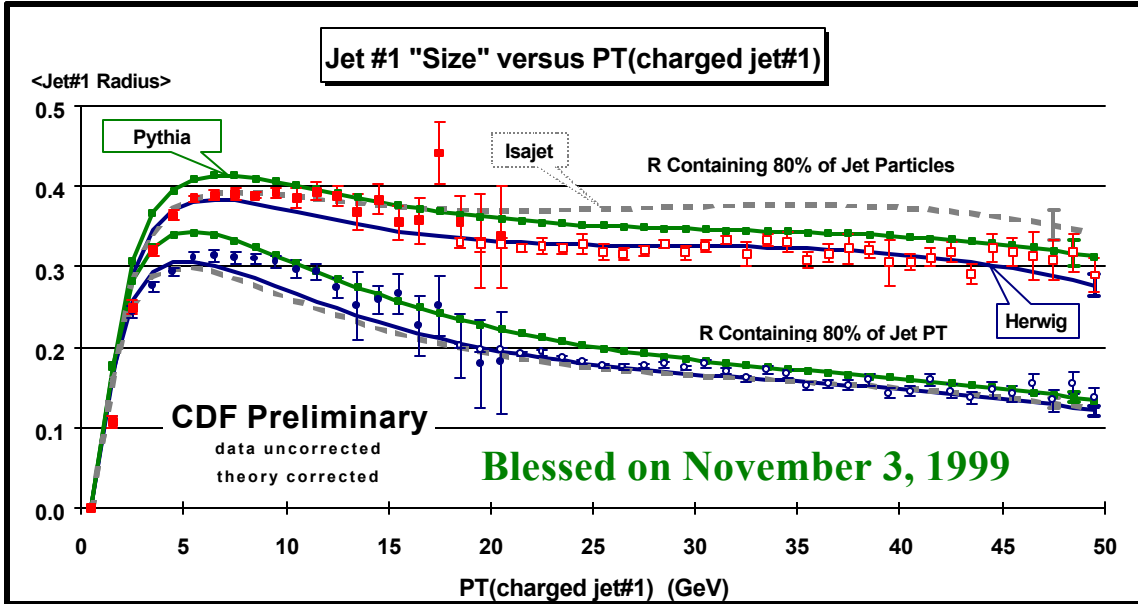


Fig. 5. Plot shows the average radius in  $\eta$ - $\phi$  space containing 80% of the charged particles (and 80% of the charged  $P_T$ ) as a function of the transverse momentum of the leading charged jet. The errors on the (*uncorrected*) data include both statistical and correlated systematic uncertainties. The QCD “hard scattering” theory curves (Herwig 5.9, Isajet 7.32, Pythia 6.115) are corrected for the track finding efficiency and have an error (*statistical plus systematic*) of around 5%.

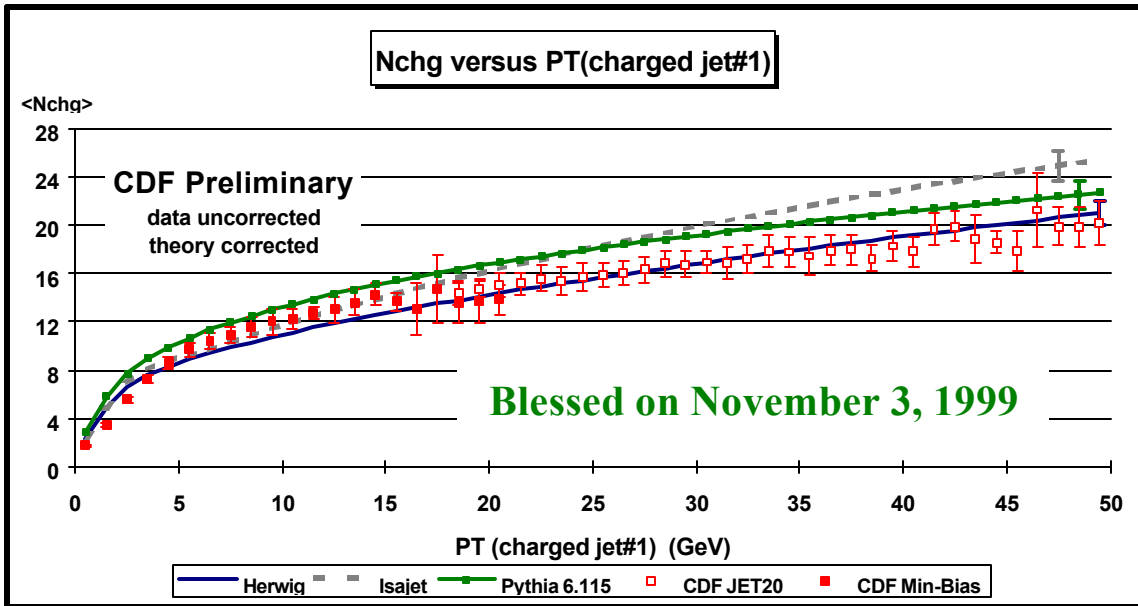
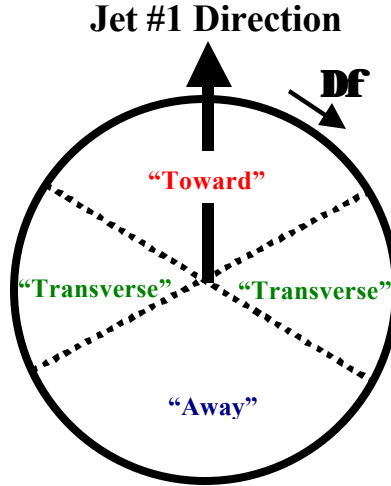
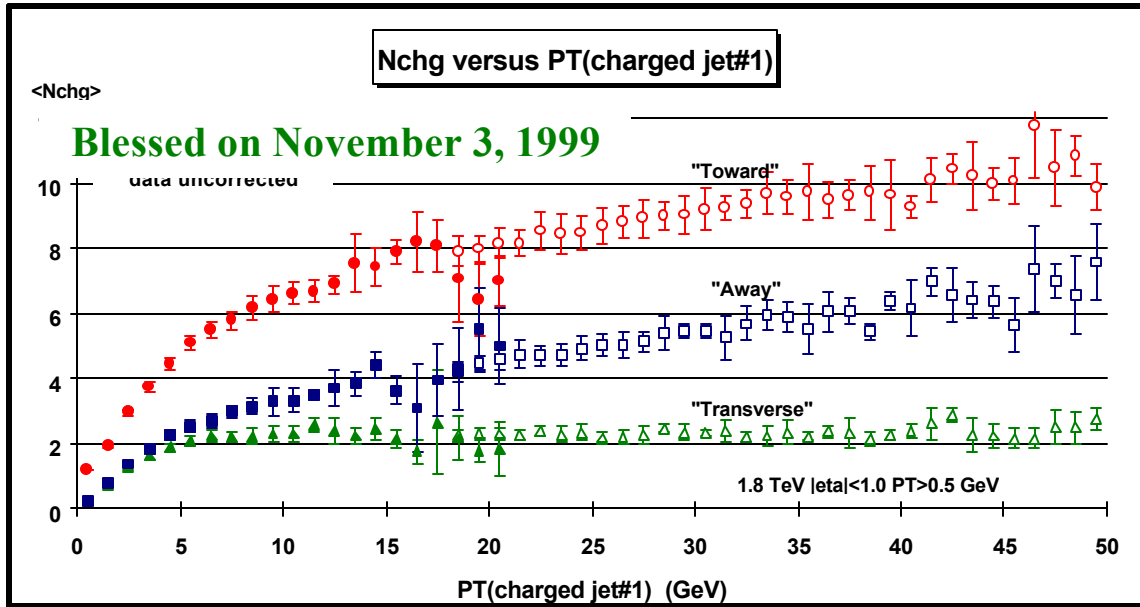


Fig. 6. Plot shows the average total number charged particles in the event ( $P_T > 0.5$  GeV,  $|\eta| < 1$  including jet#1) as a function of the transverse momentum of the leading charged jet. The solid (open) points are the Min-Bias (JET20) data. The errors on the (*uncorrected*) data include both statistical and correlated systematic uncertainties. The QCD “hard scattering” theory curves (Herwig 5.9, Isajet 7.32, Pythia 6.115) are corrected for the track finding efficiency and have an error (*statistical plus systematic*) of around 5%.



**Fig. 7.** Illustration of correlations in azimuthal angle  $\Delta\phi$  relative to the direction of the leading charged jet in the event, jet#1. The angle  $\Delta\phi = |\phi - \phi_{jet\#1}|$  is the relative azimuthal angle between charged particles and the direction of jet#1. The region  $|\Delta\phi| < 60^\circ$  is referred to as “toward” jet#1 (includes particles in jet#1) and the region  $|\Delta\phi| > 120^\circ$  is called “away” from jet#1. The “transverse” to jet#1 region is defined by  $60^\circ < |\Delta\phi| < 120^\circ$ . Each region, “toward”, “transverse”, and “away” covers the same range  $|\Delta\eta| \times |\Delta\phi| = 2 \times 120^\circ$ . Plots of  $\langle N_{chg} \rangle$  and  $\langle PT_{sum} \rangle$  as a function of  $\Delta\phi$  are referred to as “multiplicity flow in  $\phi$ ” relative to jet#1 and “transverse momentum flow in  $\phi$ ” relative to jet#1, respectively.



**Fig. 8.** The average number of “toward” ( $|\Delta\phi| < 60^\circ$ ), “transverse” ( $60^\circ < |\Delta\phi| < 120^\circ$ ), and “away” ( $|\Delta\phi| > 120^\circ$ ) charged particles ( $PT > 0.5$  GeV,  $|\eta| < 1$  including jet#1) as a function of the transverse momentum of the leading charged jet. Each point corresponds to the  $\langle N_{chg} \rangle$  in a 1 GeV bin. The solid (open) points are the Min-Bias (JET20) data. The errors on the (uncorrected) data include both statistical and correlated systematic uncertainties. The “toward”, “transverse”, and “away” regions are defined in Fig. 7.

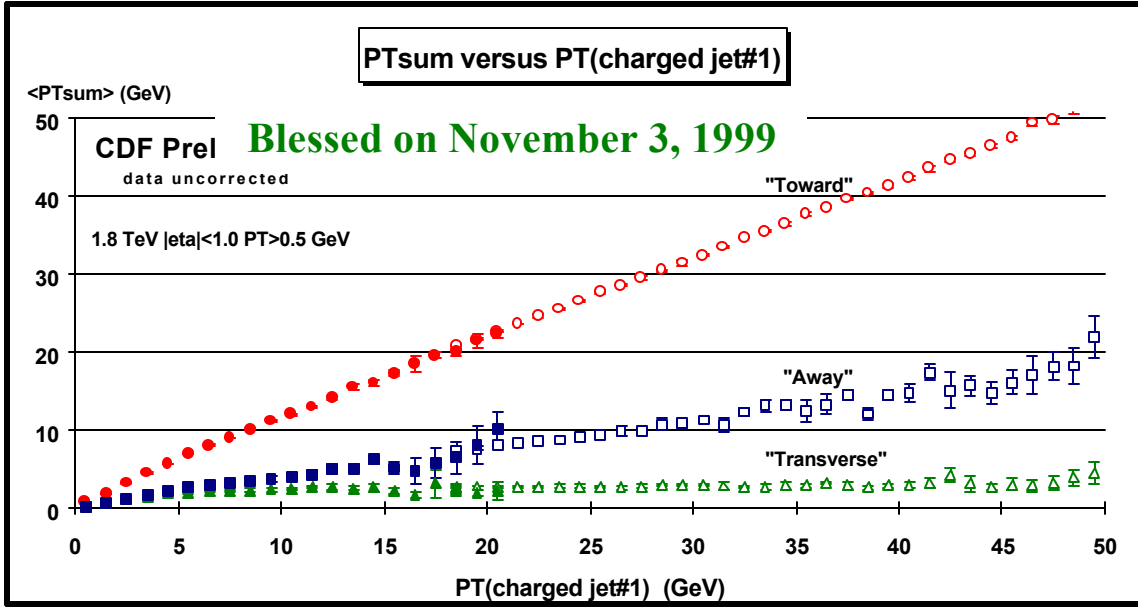


Fig. 9. The average scalar  $P_T$  sum of “toward” ( $|\Delta\phi| < 60^\circ$ ), “transverse” ( $60 < |\Delta\phi| < 120^\circ$ ), and “away” ( $|\Delta\phi| > 120^\circ$ ) charged particles ( $P_T > 0.5$  GeV,  $|\eta| < 1$  including jet#1) as a function of the transverse momentum of the leading charged jet. Each point corresponds to the  $\langle P_T \text{ sum} \rangle$  in a 1 GeV bin. The solid (open) points are the Min-Bias (JET20) data. The errors on the (uncorrected) data include both statistical and correlated systematic uncertainties. The “toward”, “transverse”, and “away” regions are defined in Fig. 7.

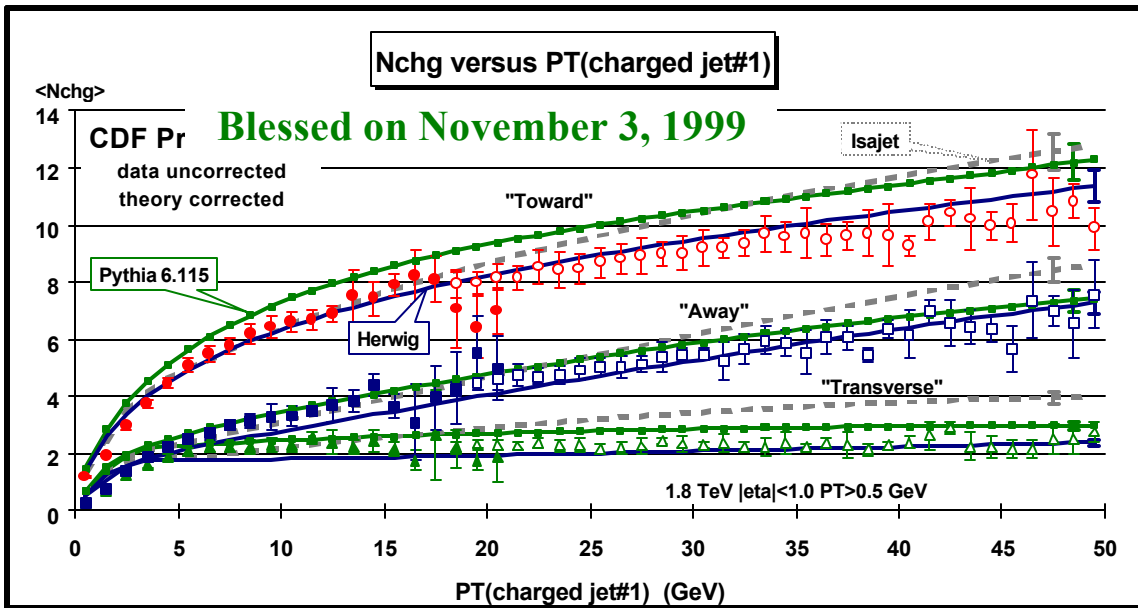


Fig. 10. Data from Fig. 8 on the average number of “toward” ( $|\Delta\phi| < 60^\circ$ ), “transverse” ( $60 < |\Delta\phi| < 120^\circ$ ), and “away” ( $|\Delta\phi| > 120^\circ$ ) charged particles ( $P_T > 0.5$  GeV,  $|\eta| < 1$  including jet#1) as a function of the transverse momentum of the leading charged jet compared to QCD “hard scattering” Monte-Carlo predictions of Herwig 5.9, Isajet 7.32, and Pythia 6.115. The errors on the (uncorrected) data include both statistical and correlated systematic uncertainties. The theory curves are corrected for the track finding efficiency and have an error (statistical plus systematic) of around 5%.

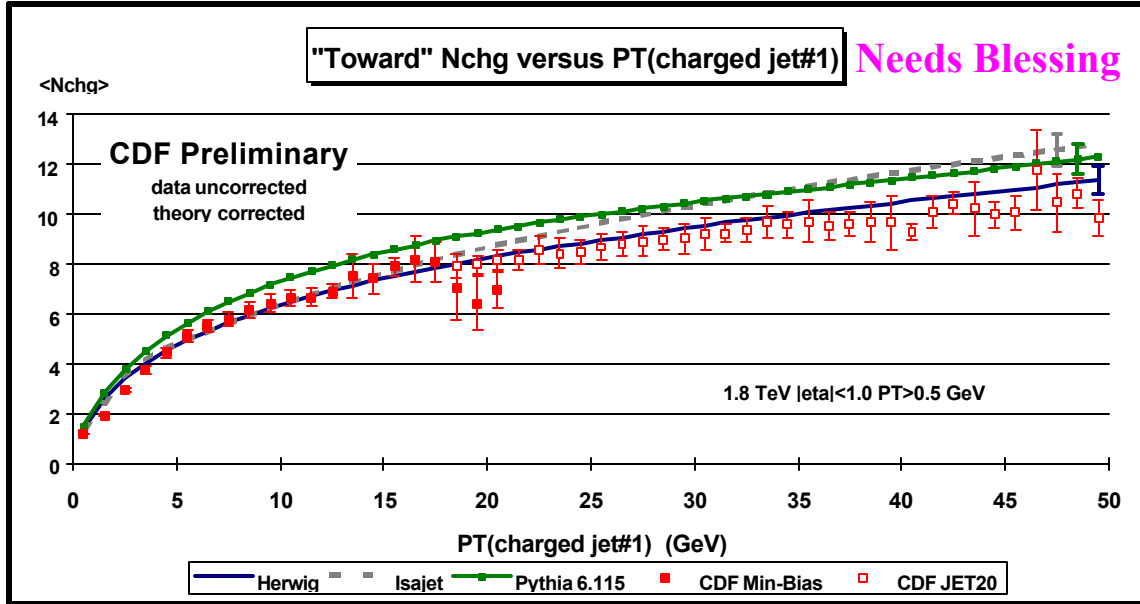


Fig. 11. Data from Fig. 8 on the average number of charged particles ( $P_T > 0.5$  GeV and  $|\eta| < 1$ ) as a function of  $P_T$  (jet#1) (*leading charged jet*) for the “toward” region” defined in Fig. 7 compared with the QCD “hard scattering” Monte-Carlo predictions of Herwig 5.9, Isajet 7.32, and Pythia 6.115. Each point corresponds to the “toward”  $\langle N_{chg} \rangle$  in a 1 GeV bin. The errors on the (*uncorrected*) data include both statistical and correlated systematic uncertainties. The theory curves are corrected for the track finding efficiency and have an error (*statistical plus systematic*) of around 5%.

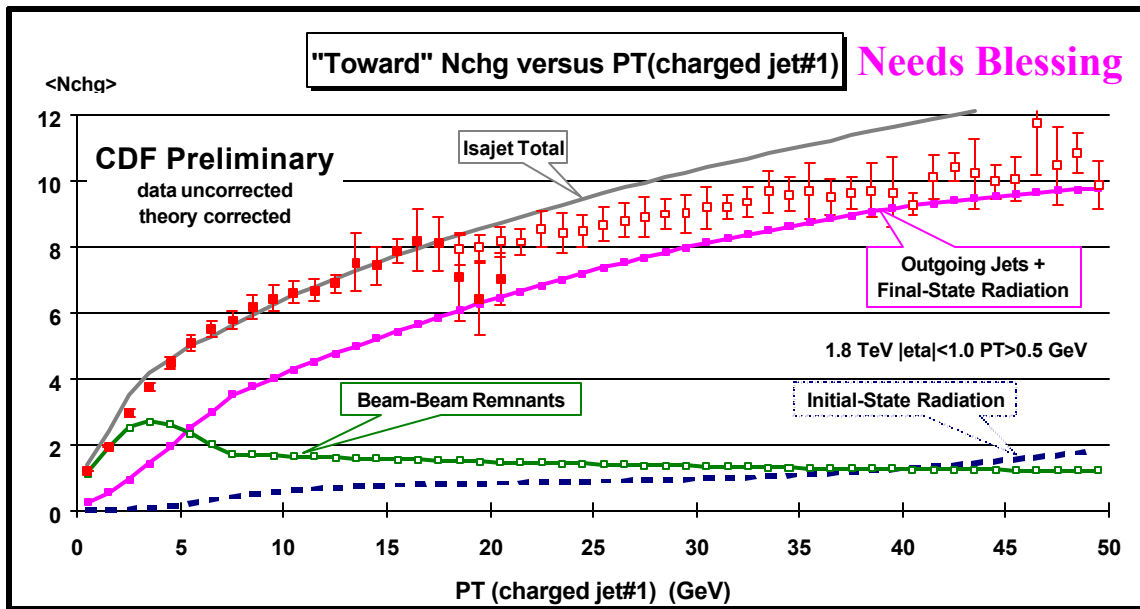


Fig. 12. Data from Fig. 8 on the average number of charged particles ( $P_T > 0.5$  GeV and  $|\eta| < 1$ ) as a function of  $P_T$ (jet#1) (*leading charged jet*) for the “toward” region defined in Fig. 7 compared with the QCD “hard scattering” Monte-Carlo predictions of Isajet 7.32. The predictions of Isajet are divided into three categories: charged particles that arise from the break-up of the beam and target (*beam-beam remnants*), charged particles that arise from initial-state radiation, and charged particles that result from the outgoing jets plus final-state radiation (see Fig. 1). The errors on the (*uncorrected*) data include both statistical and correlated systematic uncertainties. The theory curves are corrected for the track finding efficiency and have an error (*statistical plus systematic*) of around 5%.

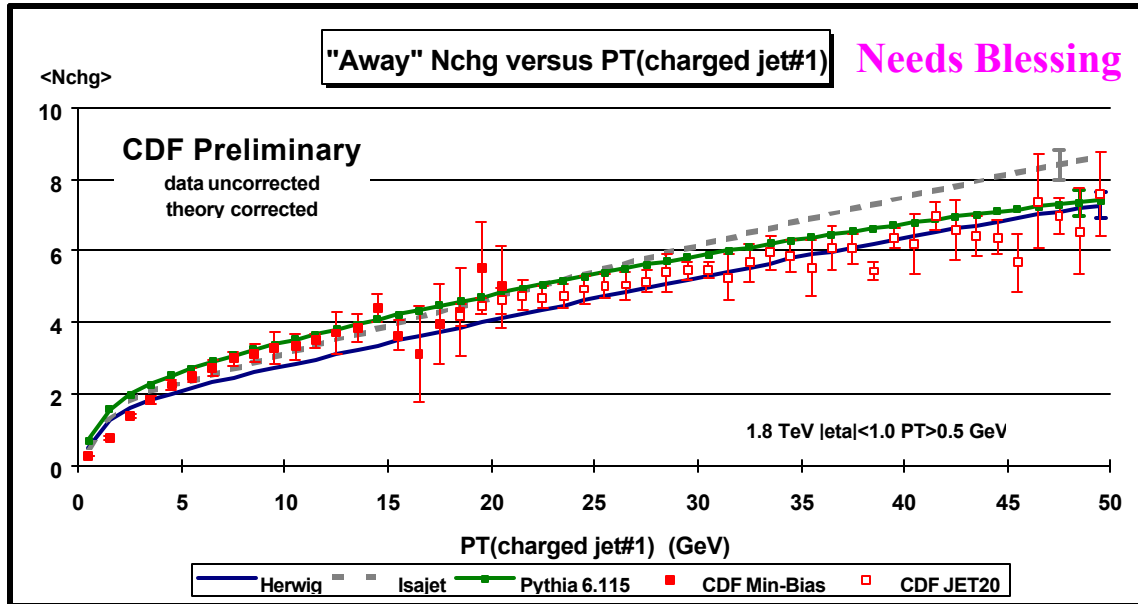


Fig. 13. Data from Fig. 8 on the average number of charged particles ( $P_T > 0.5$  GeV and  $|\eta| < 1$ ) as a function of  $P_T(\text{jet\#1})$  (*leading charged jet*) for the “away” region defined in Fig. 7 compared with the QCD “hard scattering” Monte-Carlo predictions of Herwig 5.9, Isajet 7.32, and Pythia 6.115. The errors on the (*uncorrected*) data include both statistical and correlated systematic uncertainties. The theory curves are corrected for the track finding efficiency and have an error (*statistical plus systematic*) of around 5%.

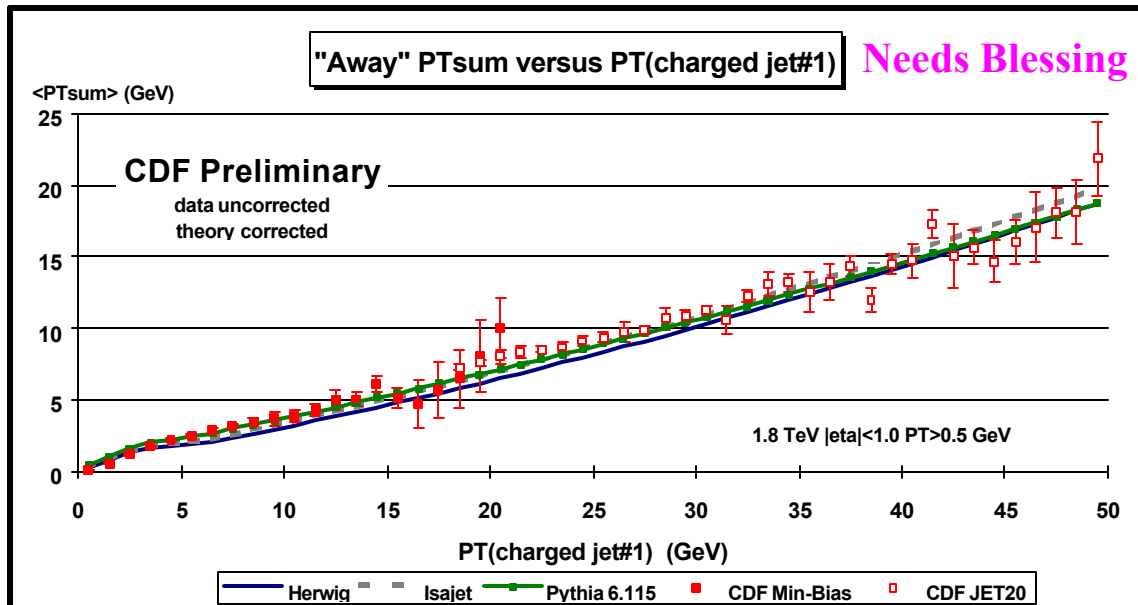
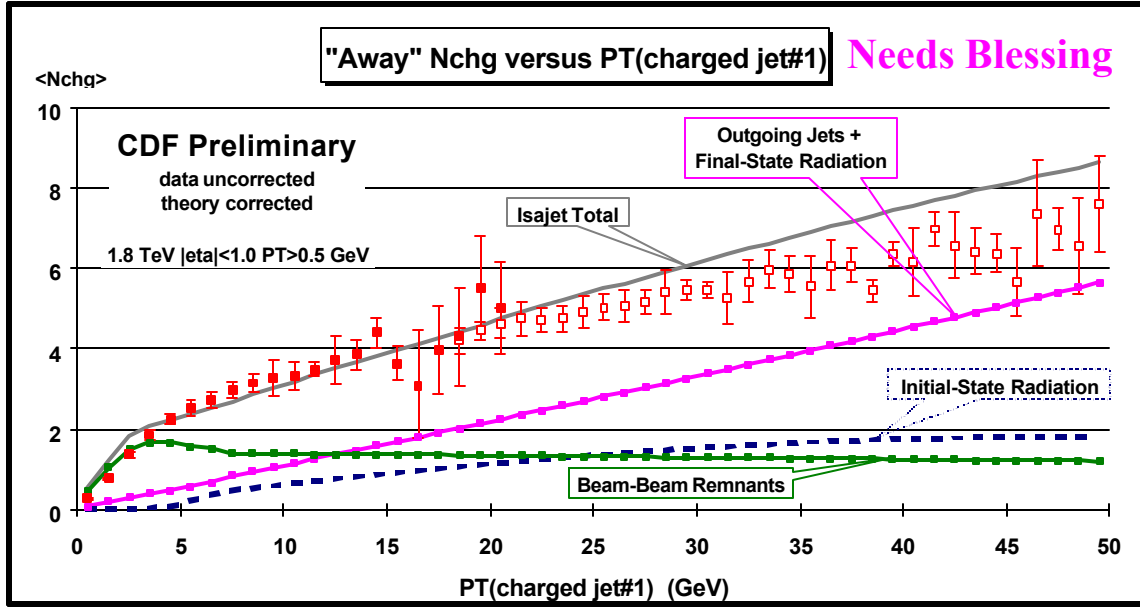
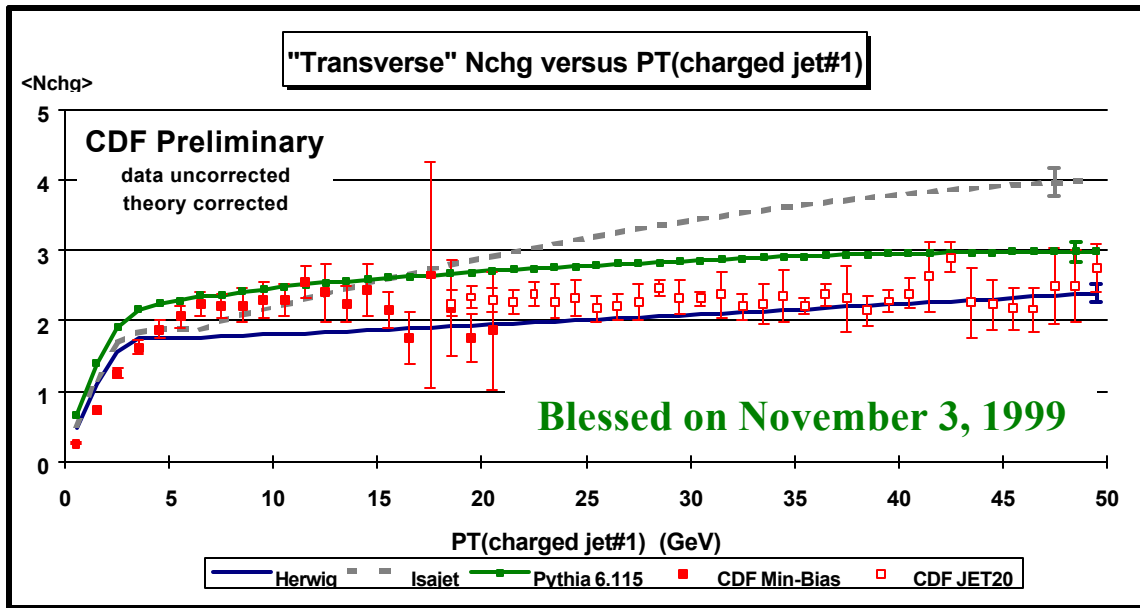


Fig. 14. Data from Fig. 9 on the average *scalar*  $P_T$  sum of charged particles ( $P_T > 0.5$  GeV and  $|\eta| < 1$ ) as a function of  $P_T(\text{jet\#1})$  (*leading charged jet*) for the “away” region defined in Fig. 7 compared with the QCD “hard scattering” Monte-Carlo predictions of Herwig 5.9, Isajet 7.32, and Pythia 6.115. The errors on the (*uncorrected*) data include both statistical and correlated systematic uncertainties. The theory curves are corrected for the track finding efficiency and have an error (*statistical plus systematic*) of around 5%.



**Fig. 15.** Data from Fig. 8 on the average number of charged particles ( $P_T > 0.5$  GeV and  $|\eta| < 1$ ) as a function of  $P_T(\text{jet}\#1)$  (*leading charged jet*) for the “away” region defined in Fig. 7 compared with the QCD “hard scattering” Monte-Carlo predictions of Isajet 7.32. The predictions of Isajet are divided into three categories: charged particles that arise from the break-up of the beam and target (*beam-beam remnants*), charged particles that arise from initial-state radiation, and charged particles that result from the outgoing jets plus final-state radiation (see Fig. 1). The errors on the (*uncorrected*) data include both statistical and correlated systematic uncertainties. The theory curves are corrected for the track finding efficiency and have an error (*statistical plus systematic*) of around 5%.



**Fig. 16.** Data from Fig. 8 on the average number of charged particles ( $P_T > 0.5$  GeV and  $|\eta| < 1$ ) as a function of  $P_T(\text{jet}\#1)$  (*leading charged jet*) for the “transverse” region defined in Fig. 7 compared with the QCD “hard scattering” Monte-Carlo predictions of Herwig 5.9, Isajet 7.32, and Pythia 6.115. The errors on the (*uncorrected*) data include both statistical and correlated systematic uncertainties. The theory curves are corrected for the track finding efficiency and have an error (*statistical plus systematic*) of around 5%.

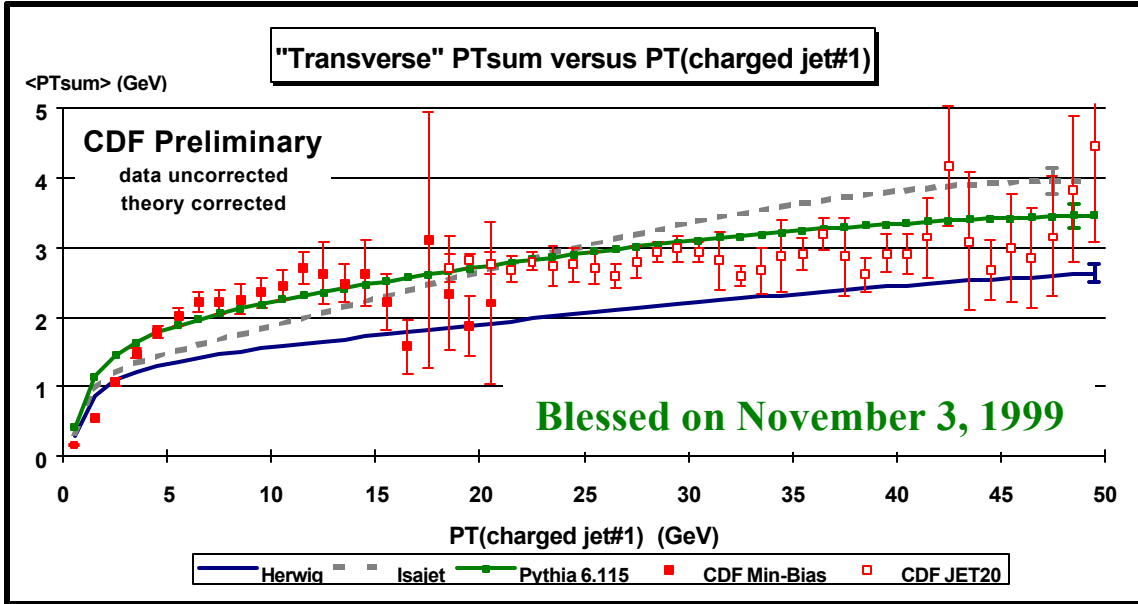


Fig. 17. Data from Fig. 9 on the average scalar  $P_T$  sum of charged particles ( $P_T > 0.5$  GeV and  $|\eta| < 1$ ) as a function of  $P_T(\text{jet}\#1)$  (leading charged jet) for the “transverse” region defined in Fig. 7 compared with the QCD “hard scattering” Monte-Carlo predictions of Herwig 5.9, Isajet 7.32, and Pythia 6.115. The errors on the (uncorrected) data include both statistical and correlated systematic uncertainties. The theory curves are corrected for the track finding efficiency and have an error (statistical plus systematic) of around 5%.

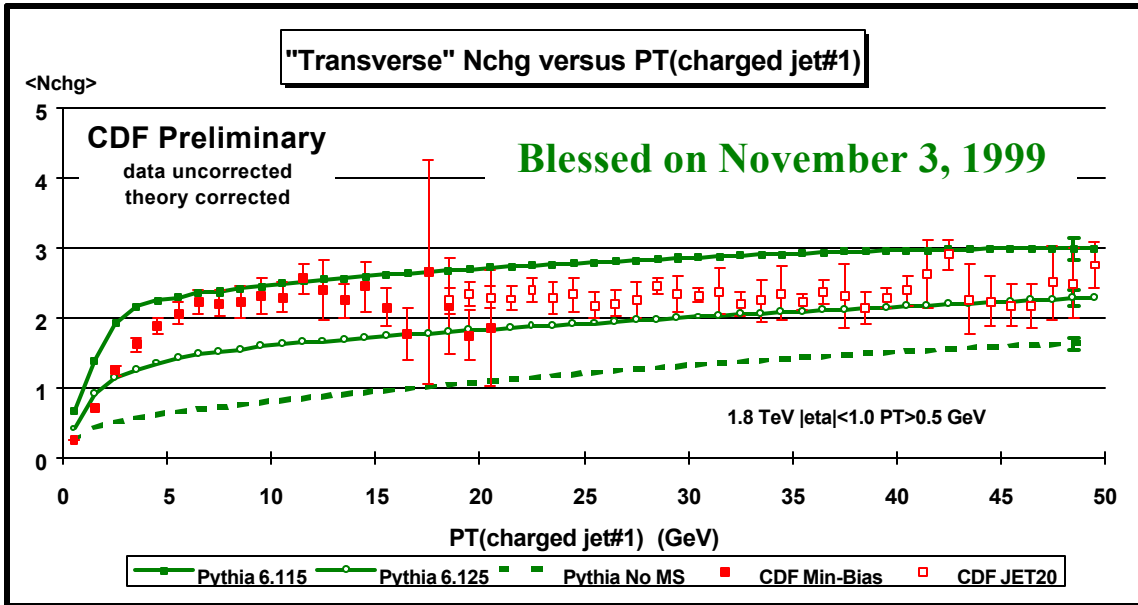


Fig. 18. Data from Fig. 8 on the average number of charged particles ( $P_T > 0.5$  GeV and  $|\eta| < 1$ ) as a function of  $P_T(\text{jet}\#1)$  (leading charged jet) for the “transverse” region defined in Fig. 7 compared with the QCD “hard scattering” Monte-Carlo predictions of Pythia 6.115, Pythia 6.125, and Pythia with no multiple parton scattering (No MS). The errors on the (uncorrected) data include both statistical and correlated systematic uncertainties. The theory curves are corrected for the track finding efficiency and have an error (statistical plus systematic) of around 5%.

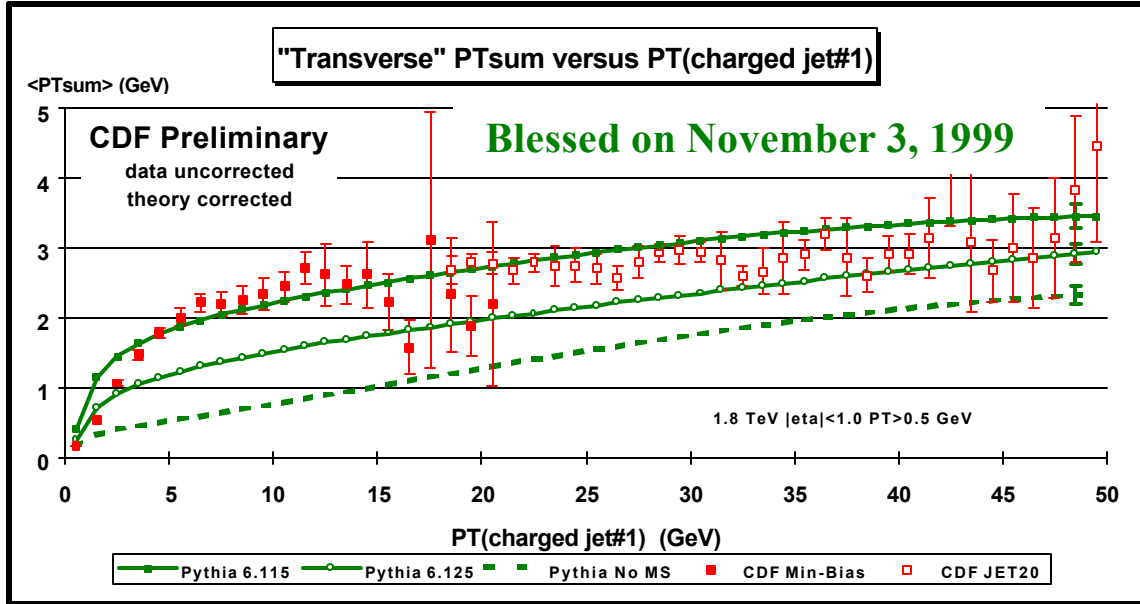


Fig. 19. Data from Fig. 9 on the average  $scalar P_T$  sum of charged particles ( $P_T > 0.5$  GeV and  $|\eta| < 1$ ) as a function of  $P_T(jet\#1)$  (*leading charged jet*) for the “transverse” region defined in Fig. 7 compared with the QCD “hard scattering” Monte-Carlo predictions of Pythia 6.115, Pythia 6.125, and Pythia with no multiple parton scattering (No MS). The errors on the (*uncorrected*) data include both statistical and correlated systematic uncertainties. The theory curves are corrected for the track finding efficiency and have an error (*statistical plus systematic*) of around 5%.

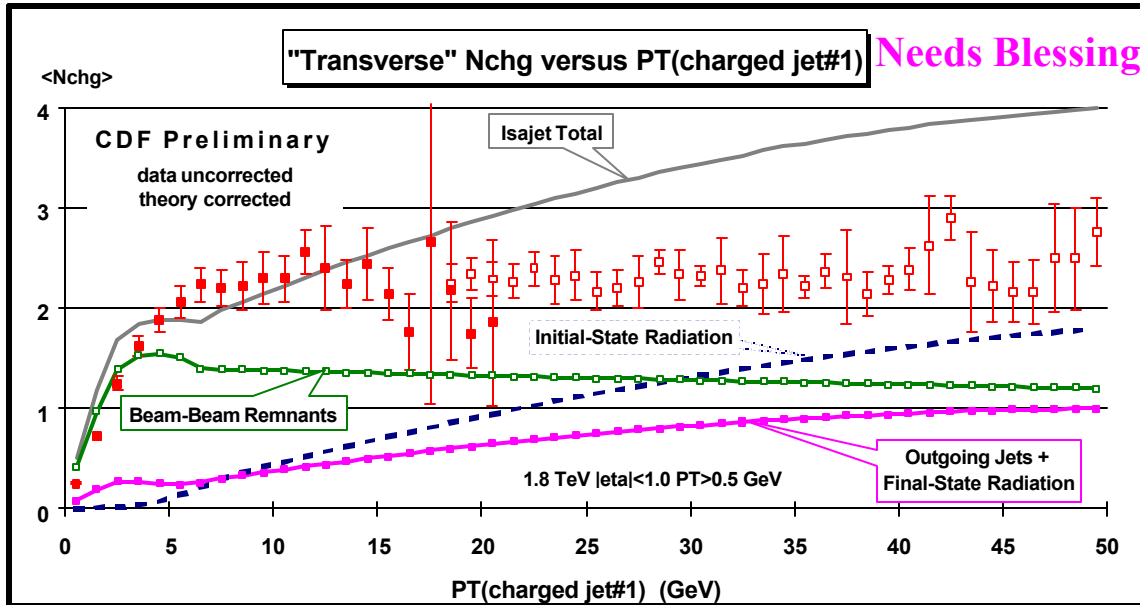


Fig. 20. Data from Fig. 8 on the average number of charged particles ( $P_T > 0.5$  GeV and  $|\eta| < 1$ ) as a function of  $P_T(jet\#1)$  (*leading charged jet*) for the “transverse” region defined in Fig. 7 compared with the QCD “hard scattering” Monte-Carlo predictions of Isajet 7.32. The predictions of Isajet are divided into three categories: charged particles that arise from the break-up of the beam and target (*beam-beam remnants*), charged particles that arise from initial-state radiation, and charged particles that result from the outgoing jets plus final-state radiation (see Fig. 1). The errors on the (*uncorrected*) data include both statistical and correlated systematic uncertainties. The theory curves are corrected for the track finding efficiency and have an error (*statistical plus systematic*) of around 5%.

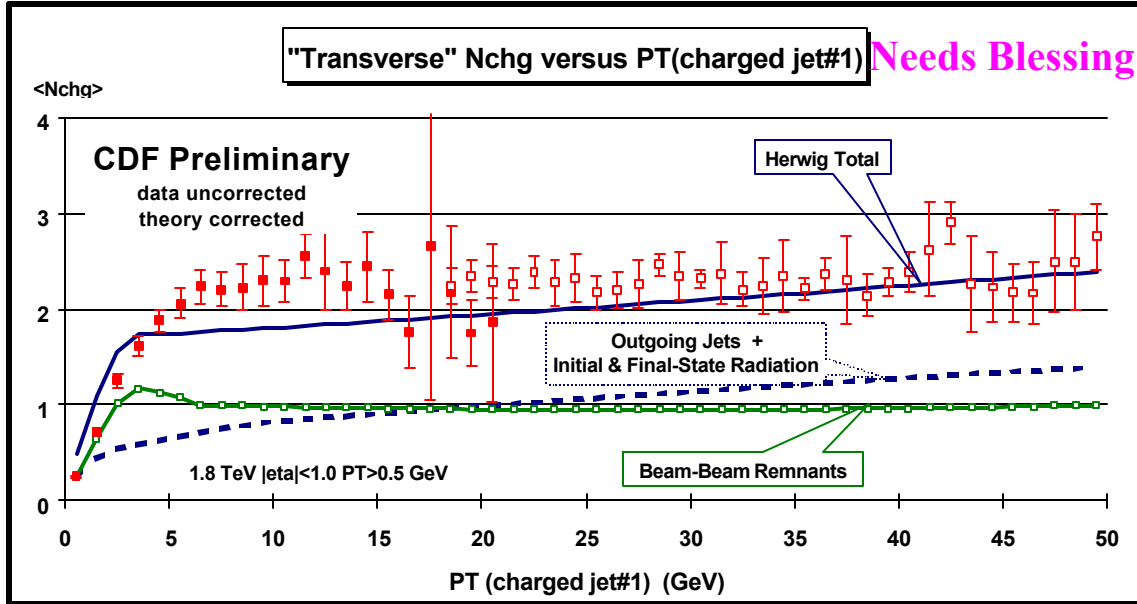


Fig. 21. Data from Fig. 8 on the average number of charged particles ( $P_T > 0.5$  GeV and  $|\eta| < 1$ ) as a function of  $P_T(\text{jet}\#1)$  (*leading charged jet*) for the “transverse” region defined in Fig. 7 compared with the QCD “hard scattering” Monte-Carlo predictions of Herwig 5.9. The predictions of Herwig are divided into two categories: charged particles that arise from the break-up of the beam and target (*beam-beam remnants*), and charged particles that result from the outgoing jets plus initial and final-state radiation (*hard scattering component*) (see Fig. 1). The errors on the (*uncorrected*) data include both statistical and correlated systematic uncertainties. The theory curves are corrected for the track finding efficiency and have an error (*statistical plus systematic*) of around 5%.

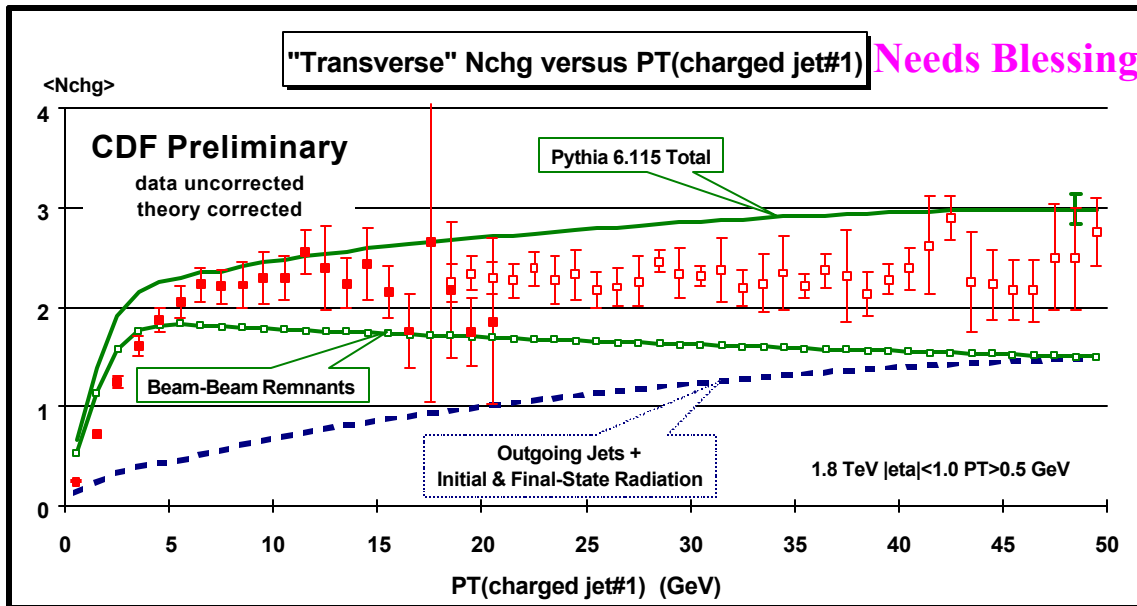


Fig. 22. Data from Fig. 8 on the average number of charged particles ( $P_T > 0.5$  GeV and  $|\eta| < 1$ ) as a function of  $P_T(\text{jet}\#1)$  (*leading charged jet*) for the “transverse” region defined in Fig. 7 compared with the QCD “hard scattering” Monte-Carlo predictions of Pythia 6.115. The predictions of Pythia are divided into two categories: charged particles that arise from the break-up of the beam and target (*beam-beam remnants*), and charged particles that result from the outgoing jets plus initial and final-state radiation (*hard scattering component*). For Pythia the beam-beam remnants include contributions from multiple parton scattering (see Fig. 2). The errors on the (*uncorrected*) data include both statistical and correlated systematic uncertainties. The theory curves are corrected for the track finding efficiency and have an error (*statistical plus systematic*) of around 5%.

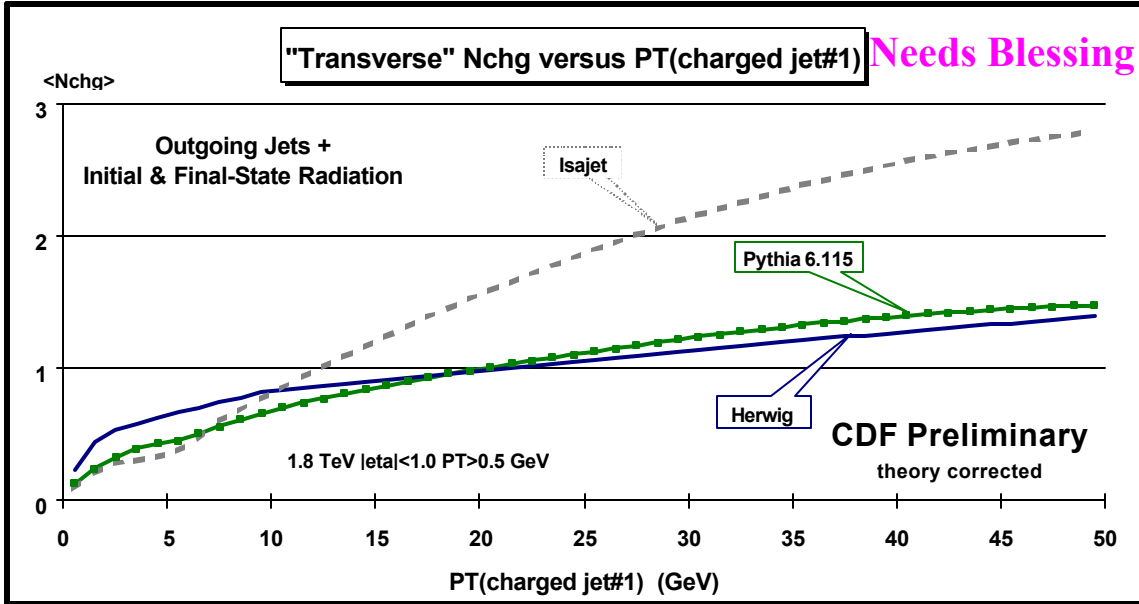


Fig. 23. QCD “hard scattering” Monte-Carlo predictions from Herwig 5.9, Isajet 7.32, and Pythia 6.115 of the average number of charged particles ( $P_T > 0.5$  GeV and  $|\eta| < 1$ ) as a function of  $P_T(\text{jet}\#1)$  (*leading charged jet*) for the “transverse” region defined in Fig. 7 arising from the outgoing jets plus initial and final-state radiation (*hard scattering component*). The curves are corrected for the track finding efficiency and have an error (*statistical plus systematic*) of around 5%.

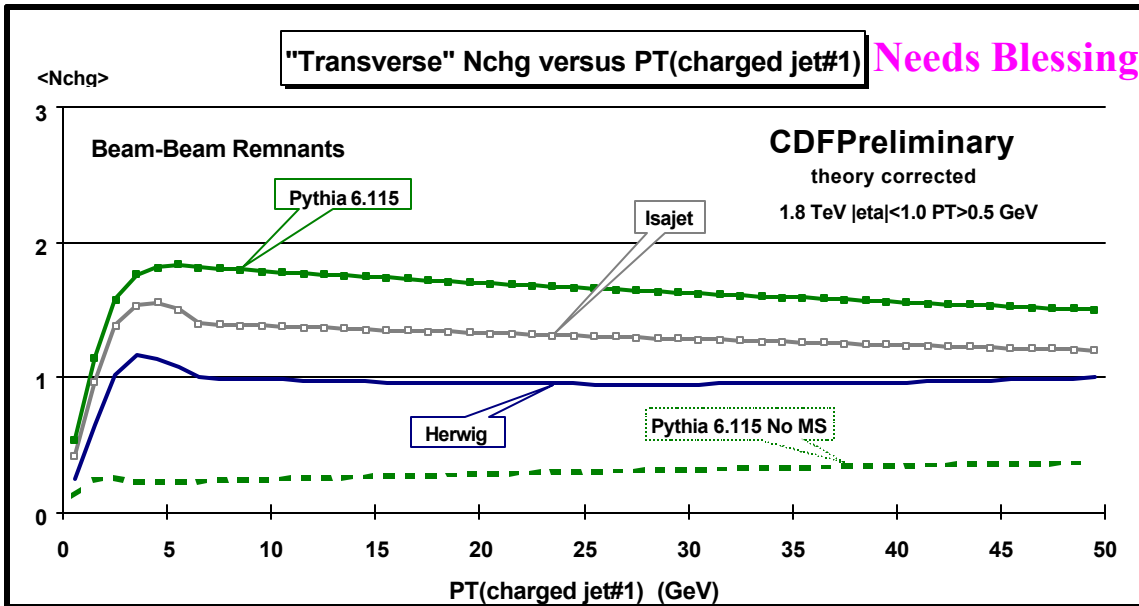


Fig. 24. QCD “hard scattering” Monte-Carlo predictions from Herwig 5.9, Isajet 7.32, Pythia 6.115, and Pythia with no multiple parton scattering (No MS) of the average number of charged particles ( $P_T > 0.5$  GeV and  $|\eta| < 1$ ) as a function of  $P_T(\text{jet}\#1)$  (*leading charged jet*) for the “transverse” region defined in Fig. 7 arising from the break-up of the beam and target (*beam-beam remnants*). For Pythia the beam-beam remnants include contributions from multiple parton scattering (see Fig. 2). The curves are corrected for the track finding efficiency and have an error (*statistical plus systematic*) of around 5%.